Facile Aerosol Route to Hollow CuO Spheres and its Superior Performance as an Oxidizer in Nanoenergetic Gas Generators

*Guoqiang Jian, Lu Liu, and Michael R. Zachariah**

Thermochemical metal/metal oxide redox reactions have twice the energy density of 2,4,6-trinitrotoluene (TNT). They suffer, however, from low pressure-volume work due to low gas expansion from the reaction. This study focuses on the development of a nanocomposite that delivers a high energy density and the potential of rapid gas release. Hollow CuO spheres with nanosized building blocks are fabricated using a "droplet-to-particle" aerosol spray pyrolysis method with the introduction of gas-blowing agents in the synthesis procedure. Nanoaluminum with hollow CuO as an oxidizer ignites in a very violent manner and exhibits excellent gas-generation behavior, demonstrating a high pressurization rate of 0.745 MPa μs^{-1} and a transient peak pressure of 0.896 MPa with a charge density of 1 mg cm^{-3}, as well as a rapid oxygen release. Compared with wet-chemistry methods, gas-phase processes are relatively low cost, nominally offer a higher purity product, and are usually configured as continuous production processes, with a limited number of steps. The synthesis strategy demonstrated is simple and should be extendable to the preparation of other hollow metal oxide structures.

1. Introduction

Hollow metal oxide micro/nanostructures are of interest for their potential applications in catalysis, nano-/microreactors, energy storage and conversion, drug delivery, and chemical sensors.[1–7] Several methods have been employed to fabricate hollow metal oxide structures, which can be broadly classified as templating and template-free methods.[1–3,8,9] Although hard-template methods are effective in producing well-defined structures, the synthetic procedures can be complex and involve a template-removal step. Recently, processes based on Ostwald ripening have been employed as a template-free strategy to produce metal oxide hollow structures,[3] through an "inside-out" mechanism.[10,11] In this approach, nanocrystallites in the core of colloidal aggregate, which are energetically less stable, dissolve, diffuse out, and redeposit to the outer surface, leading to a continuous evacuation of the core materials and the formation of the hollow structure. Compared with wet-chemistry methods, gas-phase processes are relatively low cost, nominally offer a higher purity product, and usually are configured as continuous production processes, with a limited number of steps. In fact, many modifications of gas-phase methods including chemical vapor deposition, sputtering, microplasma synthesis, combustion and flame, and aerosol/spray pyrolysis have been developed and aim to achieve large-scale industrial production of nanoparticles.[12–16] Among these methods, aerosol/spray pyrolysis offers the advantages of simplicity, high purity, relatively low cost, environmental friendliness, and continuous production.[15,16]

Nanoenergetic materials, or so called nanothermites, a subset of metastable intermolecular composites (MIC), are a relatively new class of energetic materials comprising a metallic fuel, and an oxidizer at the nanoscale that can rapidly release heat and pressure. They have found application as propellants and explosives, as well as in propulsion power in micro-/nanoelectromechanical systems (MEMS/NEMS).[17–19] In most formulations, aluminum is employed as the fuel because of its high reaction enthalpy and ready availability, and low-cost metal oxides such as CuO and Fe_2O_3 are commonly used as oxidizers (Equation 1):[17]

$$Al + \frac{3}{2}MO \rightarrow \frac{1}{2}Al_2O_3 + \frac{3}{2}M + \Delta H \quad (1)$$

In nanoenergetic-material formulations, the use of nanoparticles is primarily used as a means to reduce diffusion lengths between reactive components, and to increase the contact area between the fuel and the oxidizer. As a result, an enhanced flame-propagation rate of the wave front and energy-release rate of the nanoenergetic materials (up to three orders of magnitude) can be achieved, compared with their corresponding microsized formulations.[20] Moreover, it has been demonstrated that increasing the interfacial contact area between the oxidizer and the fuel at the nanoscale can significantly improve the performance of nanoenergetic formulations.[21–24] In particular, Al/CuO has been found to be a very vigorous formulation

G. Q. Jian, L. Liu, Prof. M. R. Zachariah
Department of Chemistry and Biochemistry
University of Maryland
College Park, MD 20742, USA
E-mail: mrz@umd.edu
Prof. M. R. Zachariah
Department of Mechanical Engineering
University of Maryland
College Park, MD 20742, USA

DOI: 10.1002/adfm.201202100

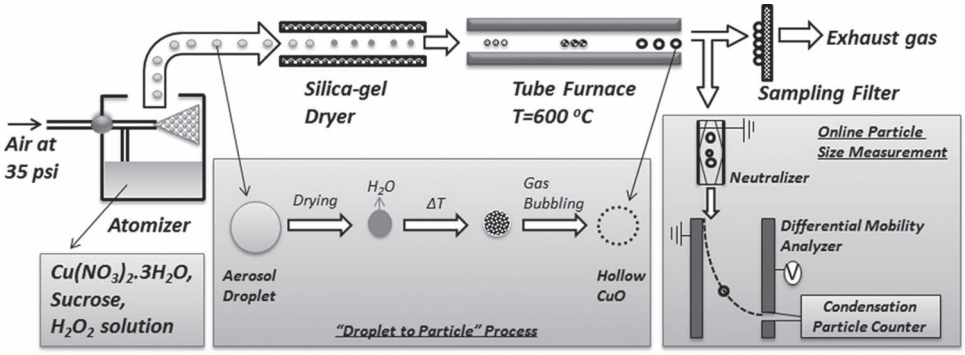

Scheme 1. Illustration of aerosol spray pyrolysis route to hollow CuO spheres and online particle-size measurement system.

that can rapidly release a large amount of gaseous products and will be the subject of this paper.[25–27]

In the present study, we focus on developing an Al/CuO nanocomposite that can deliver a high energy density, and with the potential of rapid gas release. For this purpose, we have developed a novel and facile approach to fabricate hollow CuO spheres by a "droplet-to-particle" aerosol spray pyrolysis route. In particular, the shells of hollow CuO spheres were found to comprise ≈10 nm CuO nanoparticles as building blocks, indicating their potential large interfacial contact with fuel nanoparticles when forming a nanocomposite with aluminum nanoparticles. The energetic performance of the as-prepared nanocomposites that contained hollow CuO spheres was then tested for their combustion behavior and enhanced performance was found.

2. Results and Discussion

2.1. Hollow-CuO-Sphere Synthesis and Characterization

A schematic illustration for the preparation and online particle-size measurement of hollow CuO nanospheres is presented in **Scheme 1**. The process is a "droplet-to-particle" aerosol spray pyrolysis approach, whereby precursor solutions are atomized and decomposed thermally to form particles. The key to the formation of the hollow CuO structure with small nanoparticles as building blocks is the introduction of sucrose and hydrogen peroxide (H_2O_2) to the copper nitrate starting solution as an in situ blowing agent. As shown in Scheme 1, online particle-size characterization is used to obtain the size distribution of the product particles.

Scanning electron microscopy (SEM) and transmission electron microscopy (TEM) images, (**Figure 1**a,b) show that the as-prepared particles have hollow structures comprising a thin shell with a 5–10 nm wall thickness. The High-resolution TEM (HR-TEM) image shown in Figure 1c confirms the shell of the hollow structure is actually an assembly of ≈10 nm nanoparticles. The inset lattice-fringe image shown in Figure 1c shows a crystallinity that is indexed to the monoclinic phase of CuO, which was further verified with a bulk sample from by X-ray diffraction (XRD), as shown in Figure 1e. To ensure the removal of

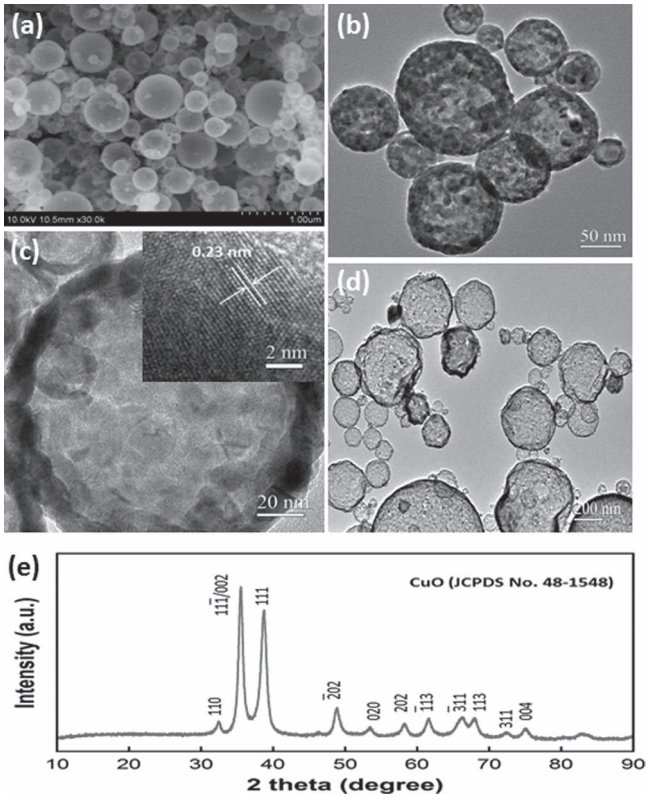

Figure 1. a–e) SEM image (a), TEM and HR-TEM images (b–d) and XRD (e) of prepared hollow CuO spheres collected from the sample filter. Note: (d) shows the TEM image of hollow CuO spheres synthesized from solution with a higher precursor concentration and more gas-blowing agents.

any carbon residue as a remnant of the sucrose, the as-collected samples were further heated in air at 350 °C for 1 h. The TEM images in **Figure 2** show no observable morphology change as compared with Figure 1b,c, indicating no phase growth occurred during heating. The XRD and the selected area electron diffraction (SAED) results in Figure 2b confirm the single phase of CuO (JCPDS No. 48–1548).

To investigate the effect of sucrose and H_2O_2 on the morphology and composition of the products, an experiment was

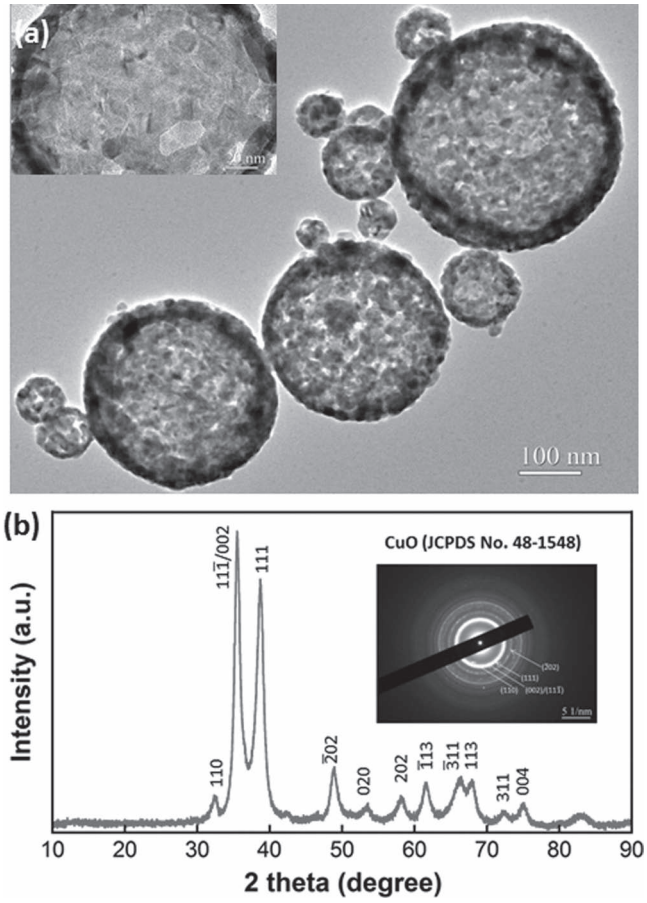

Figure 2. a,b) TEM image (a) and XRD spectrum (b) of prepared hollow CuO nanospheres after heat treatment in air (350 °C, 1 h). The inset of (a) is an HR-TEM image showing the shell and the crystallite. The inset of (b) is an SAED pattern of the hollow CuO spheres after heat treatment in air.

carried out using the same concentration of copper nitrate solution but without any sucrose and H_2O_2. In this case, product particles only show a partially hollow interior as seen in **Figure 3**a, implying that copper nitrate precursor decomposition is also acting like a blowing agent.

$$2Cu(NO_3)_2 \rightarrow 2CuO + 4NO_2 + O_2 \quad (2)$$

The XRD patterns shown in Figure 3c (XRD spectrum i) shows that the product contains CuO (JCPDS No.48–2548) and $Cu_2(OH)_3NO_3$ (JCPDS No.15–0014) phases, indicating incomplete reaction of the precursor, contrary to the addition of sucrose and H_2O_2 case (Figure 1e). Post-treatment of this sample in air at 350 °C for 1 h produces phase-pure CuO (Figure 3a, and XRD spectrum ii in Figure 3c). Prior work has shown that nitrate decomposition can be promoted by sucrose oxidation,[28] which also suggests why, even though the nitrate should have ample gas products to create a hollow, it did not. The sucrose, under the assumption of oxidation to CO_2 and water should only produce about a third as much gas as the nitrate under our conditions, but can form hollow structures because of faster gas-production kinetics (Supporting Information, Figure S1). The role of the H_2O_2 is to catalyze the oxidation of the sucrose, which is also known to rapidly polymerize into a tar-like substance in the absence of a very strong oxidizer, as shown in Figure S2a in the Supporting Information. It has been shown in Figure S2b in the Supporting Infomation that a reduced formation of carbon species occurs when adding H_2O_2 to the precursor solution. The observation that complete decomposition of the copper precursor was aided by sucrose and H_2O_2 addition seems to imply that possible exothermic reactions in the particle promote complete precursor decomposition. Based on the above observations, we conclude that the addition of a gas generator, sucrose (forming CO_2, H_2O), in addition to the inherent gas-generation properties of a nitrate salt, can promote the formation of large, thin-walled cavities in metal oxide particles.

Online particle sizing was employed with a differential mobility analyzer (DMA) system and a condensation particle counter (CPC). For these experiments, the copper nitrate concentration in the precursor solutions was fixed and the size distribution of the aerosol was determined with and without the gas-blowing agents. The distributions shown in **Figure 4** clearly show a shift in the size distribution, which peaks at ≈57 nm without the blowing agents, to ≈85 nm with the added sucrose and H_2O_2. Indeed larger hollow particles can be produced by employing higher concentrations of copper nitrate precursor and blowing agents, which can be seen in Figure 1d.

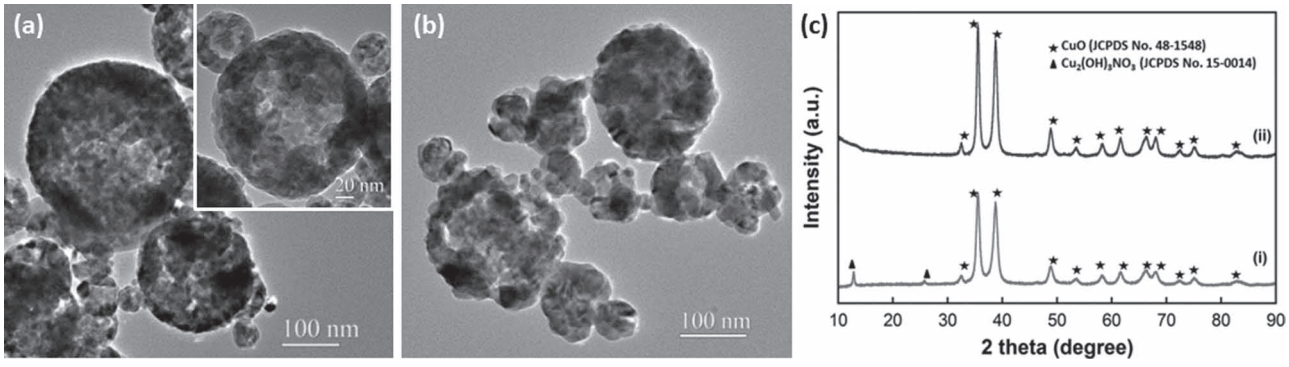

Figure 3. a,b) TEM images of the as-prepared partially hollow product from a precursor solution without sucrose and H_2O_2 (a) and after heat treatment in air at 350 °C for 1 h (b). c) Corresponding XRD spectra: i – as prepared, ii – after heat treatment.

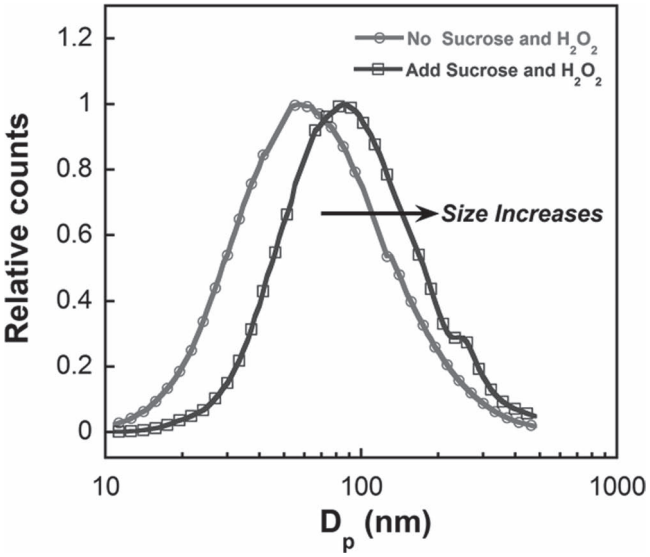

Figure 4. Particle-size distributions of CuO produced by aerosol spray pyrolysis measured using a differential mobility analyzer (DMA) coupled with a condensation particle counter (CPC).

2.2. Performance of Hollow CuO as an Oxidizer in Nanoenergetic Formulations

To evaluate the effect of this new morphology in a nanoenergtic-type application, the hollow CuO was ultrasonically mixed with aluminum nanoparticles in a stoichiometric ratio, and after drying, 12.5 mg were ignited in a combustion cell (≈13 cm^3). For comparison, the partially hollow CuO (Figure 3b) and commercial CuO nanoparticles (<50 nm, TEM image shown in Figure S3 in the Supporting Information) were also tested. **Figure 5**a shows the temporal pressure traces in the combustion cell for the various mixtures. All of the pressure traces show a rapid rise, which occurs on the order of microseconds, with the hollow CuO spheres containing thermite achieving a pressure rise of ≈0.896 MPa in only 1.2 μs, significantly outperforming the partially hollow CuO (0.496 MPa in 1.6 μs), and commercial CuO NPs (0.400 MPa in 1.6 μs). From Figure 5a, we also found that hollow CuO spheres achieve the maximum pressure value in the first 1.2 μs, while the other two reach the maximum pressure value at a much later time, 23.2 and 25.6 μs for partial hollow CuO spheres and CuO NPs respectively. Comparing the absolute pressure rise with systems that are known to have the highest pressurization rate P_{max}/t_{rise} (e.g., $KMnO_4$ nanoparticles (1.999 MPa μs^{-1} for Al/$KMnO_4$),[29] and perchlorate-containing core-shell nanostructures (0.772–2.454 MPa μs^{-1} for Al/$KClO_4$+CuO),[30] we find that these hollow CuO structures yield comparable results of ≈0.745 MPa μs^{-1}. High-speed imaging of Al/hollow CuO thermite on the fast-heating wire (≈10^6 K s^{-1}) shows a violent flame front, as shown in Figure 5c.

The corresponding optical-emission traces for all three thermite formulations are shown in Figure 5b. The burning times for all three formulations are roughly the same: full width half maximum (FWHM) = 173 μs for hollow CuO, which is much longer than the pressure rise time, suggesting that in all of the cases, the burning behavior is rate limited by the aluminum fuel, or at least is independent of the oxide morphology. The high pressurization rate of the hollow CuO spheres may be associated with their higher surface area, which is composed of very fine ≈10 nm primary particles. In essence, this is really an aggregate of the primary particles, which are sufficiently less agglomerated and thus more ready to interfacially react with the fuel. In conjunction, we explored the temporal oxygen-release kinetics from these oxidizers. Based on our previous work on

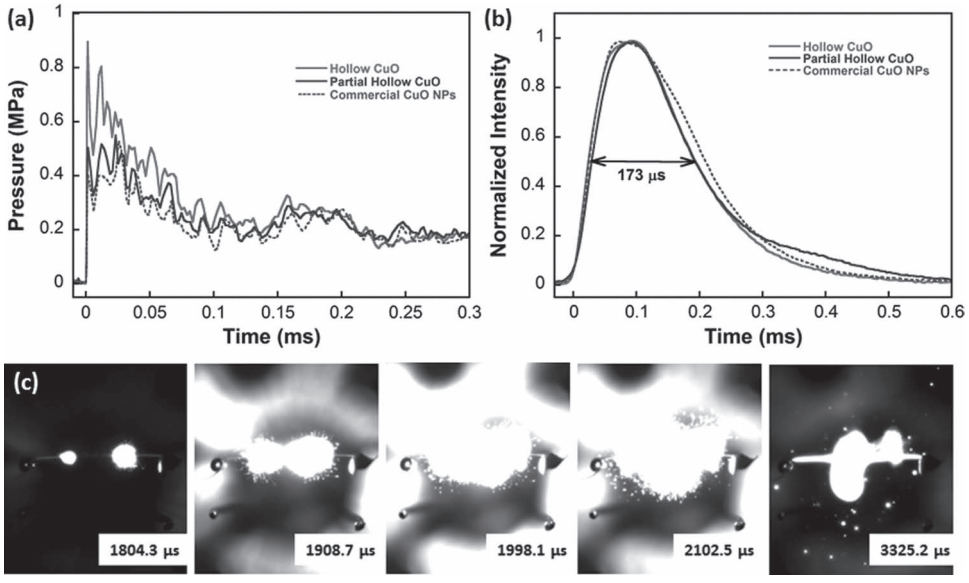

Figure 5. a,b) Pressure (a) and optical (b) traces for nanoaluminum-based thermite formulations with hollow CuO spheres (red line), partially hollow CuO (blue line), and commercial CuO nanoparticles (green line) as oxidizers in a combustion cell. c) Sequential snapshots of hollow CuO containing nanoaluminum thermite burning on a fast-heating wire. The labeled times represent the time elapsed (μs) after triggering.

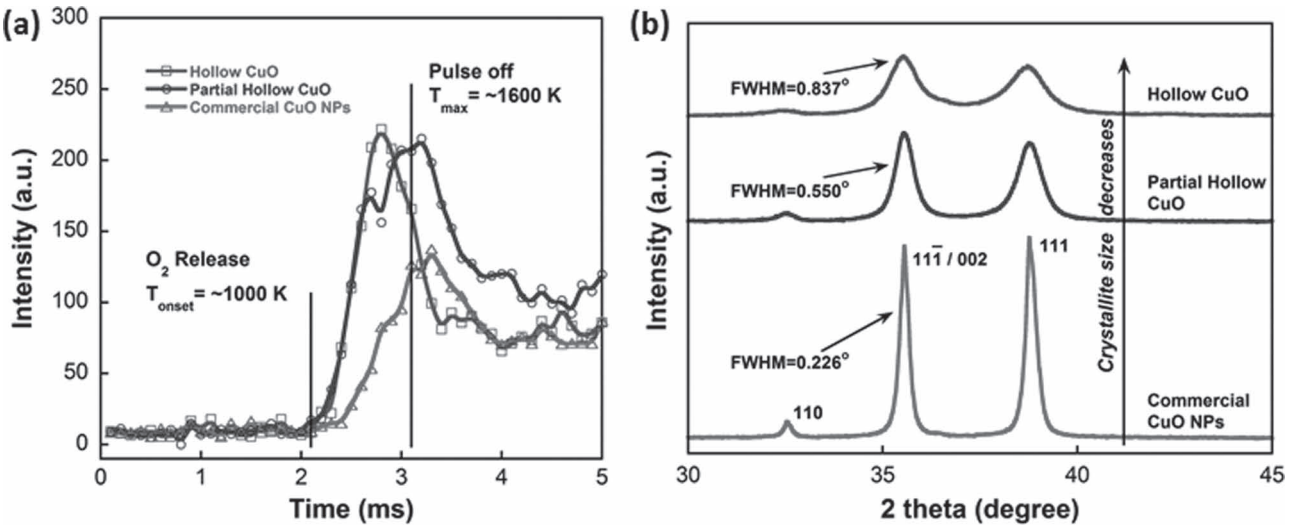

Figure 6. a) Temporal profile of oxygen release upon heating both hollow and partially hollow CuO spheres, and commercial CuO NPs (labeled as <50 nm). The heating pulse time was 3.1 ms. b) XRD spectra for hollow CuO, partially hollow CuO, and commercial CuO NPs.

oxygen-release kinetics, we expected that the faster-reacting material would release O_2 faster.[26]

To compare the oxygen release kinetics of all three CuO structures, we rapidly heated the oxidizers on a 76 μm Pt wire at a heating rate of 5×10^5 K s^{-1}. The temporal profile of oxygen release from the three CuO structures is shown in **Figure 6**a. We observed no difference in the onset temperature for oxygen release ≈1000 K. However, quite clearly the hollow CuO spheres release oxygen at a faster rate than the partially hollow material and the commercial CuO aggregated NPs. These differences in performance may be attributed to differences in the crystallite sizes of the CuO primary particle building blocks, as shown in Figure 6b. The line widths of the XRD patterns indicate differences in crystallite size, which can be estimated by the Scherrer equation, giving average crystallite sizes of 40.1 nm for commercial CuO, 16.4 nm for the partial hollow CuO, and 10.8 nm for the hollow CuO, consistent with the TEM observations. It is reasonable to expect that smaller crystallite sizes lead to a higher oxygen fugacity.[31] Additionally, we have measured a lower activation energy for oxygen release kinetics per unit mass by high-heating-rate mass spectrometry.[32] We note that the temporal profiles for the oxygen release shown in Figure 6a get wider with increasing crystallite size, and are similar to the trend observed in the combustion cell. Part of this may be attributed to the narrow primary-particle-size distribution in the hollow spheres (Figure 2a) relative to the other structures (Figure 3b).

3. Conclusions

In summary, this paper reports on the development of an Al/CuO nanocomposite which shows a better performance than previous ones adopted with nanoparticles. The hollow CuO spheres with thin shell thickness employed in the nanocomposite were prepared by a simple aerosol spray pyrolysis method with the introduction of gas-blowing agents in the synthesis procedure. The resultant hollow CuO spheres comprised small nanosized building blocks with a crystallite size of ≈10 nm. The CuO hollow spheres exhibit excellent gas-generation behavior, demonstrating a high pressurization rate of 0.745 MPa μs^{-1} and a transient peak pressure of 0.896 MPa, as well as a rapid oxygen release. The synthesis strategy demonstrated is simple and should be extendable to the preparation of other hollow metal oxide structures.

4. Experimental Section

Aerosol Spray Pyrolysis and Material Characterization: Hollow CuO spheres were prepared by an aerosol spray pyrolysis method as illustrated in Scheme 1. 0.9664 g of copper nitrate trihydrate ($Cu(NO_3)_2{\cdot}3H_2O$) (Strem Chemical), 0.1711 g of sucrose ($C_{12}H_{22}O_{11}$) (Sigma–Aldrich) and 5 mL of hydrogen peroxide solution (30 wt%. H_2O_2) (Sigma–Aldrich) were dissolved into 45 mL of water. Aerosol droplets containing the dissolved precursors were generated using compressed air at a pressure of 0.24 MPa in a collision-type atomizer. The geometric mean diameter of the droplets was measured to be ≈1 μm using a laser aerosol spectrometer. The produced aerosol droplets were passed through a silica-gel diffusion dryer to remove most of the solvent, and passed to a tube furnace at 600 °C. The normal residence time was around 1 s for a total gas flow rate of 3.5 L min^{-1}.The products were collected on a 0.4 μm (pore size) HTTP Millipore filter and further heated at 350 °C for 1 h in air to remove any possible carbon residue in the sample. As a comparison, CuO particles were also synthesized through the same process with no sucrose and H_2O_2 added to the precursor solution. Typical product yields exceeded 30%. Online particle-size measurement was obtained by using a home-built differential mobility analyzer (DMA) system and a condensation particle counter (CPC) (CPC model 3025, TSI Inc.). The materials were characterized by transmission electron microscopy (TEM) and selected area electron diffraction (SAED) (JEOL JEM 2100F), scanning electron microscopy (SEM) (Hitachi, SU-70 FEG-SEM), and powder X-ray diffraction (XRD) (Bruker D8 Advance using Cu K_α radiation).

Combustion-Cell Characterization: CuO oxidizers were mixed with aluminum nanoparticles with 70% active Al determined by TGA (Argonide Corporation, designated as 50 nm ALEX) with a stoichiometric ratio. Approximately 10 mL of hexane was then added and the thermite

mixture was ultrasonicated for 30 min to ensure intimate mixing. After the evaporation of hexane in air, the powder was then gently broken apart. A constant-volume combustion cell (≈13 cm^3) was used to measure the pressure and optical emission of thermite sample simultaneously.[27] In this study, 12.5 mg of the loose thermite sample was placed inside the combustion cell and ignited by Joule heating of a nichrome coil on top of the loose powder. One attached piezoelectric pressure transducer together with an in-line charge amplifier and signal conditioner were used to measure the pressure change. The optical signal was simultaneously collected by a lens tube assembly, containing a planoconvex lens (f = 50 mm) and a photodetector to collect the broadband emission. In comparison, commercial CuO nanoparticles (<50 nm) (Sigma–Aldrich) were also tested as an oxidizer in the combustion cell.

Time-Resolved Mass Spectrometry Measurement and High-Speed Imaging: The recently developed temperature-jump/time-of-flight mass spectrometer (T-Jump/TOFMS) was used to study the oxygen release from the CuO oxidizers.[26] Typically, a ≈10 mm-long Pt wire (76 μm) was coated with a thin layer of CuO sample powder (ultrasonicated in hexane for 30 min). The coated wire was rapidly heated to approximately 1800 K at a heating rate of 5×10^5 K s^{-1}. Time-resolved mass spectra combined with wire temperature were then used for characterization of the species produced during the rapid heating. High-speed digital-video imaging of sample combustion on the wire was conducted using a Vision Research Phantom v12.0 digital camera. The high-speed video was taken at a resolution of 256 × 256 pixels and a frame rate of 67 065 fps (14.9 μs per frame).

Supporting Information

Supporting Information is available from the Wiley Online Library or from the author.

Acknowledgements

This work was supported by the Defense Threat Reduction Agency and the Army Research Office. We acknowledge the support of the Maryland NanoCenter and its NispLab. The NispLab is supported in part by the NSF as a MRSEC Shared Experimental Facility. We would also like to thank Dr. Li-Chung Lai for helpful discussions.

Received: July 25, 2012
Revised: August 25, 2012
Published online: October 16, 2012

[1] X. W Lou, L. A. Archer, Z. C. Yang, *Adv. Mater.* **2008**, *20*, 3987.
[2] Q. Zhang, W. S. Wang, J. Goebl, Y. D. Yin, *Nano Today* **2009**, *4*, 494.
[3] J. Hu, M. Chen, X. S. Fang, L. M. Wu, *Chem. Soc. Rev.* **2011**, *40*, 5472.
[4] J. Liu, S. Z. Qiao, S. J. Chen, X. W. Lou, X. R. Xing, G. Q. Lu, *Chem. Commun.* **2011**, *47*, 12578.
[5] X. Y. Lai, J. E. Halpert, D. Wang, *Energy Environ. Sci.* **2012**, *5*, 5604.
[6] Z. Y. Wang, L. Zhou, X. W. Lou, *Adv. Mater.* **2012**, *24*, 1903.
[7] J. H. Lee, *Sensors Actuators B* **2009**, *140*, 319.
[8] Y. D. Yin, R. M. Rioux, C. K. Erdonmez, S. Hughes, G. A. Somorjai, A. P. Alivisatos, *Science* **2004**, *304*, 711.
[9] J. G. Railsback, A. C. Johnston-Peck, J. W. Wang, J. B. Tracy, *ACS Nano* **2010**, *4*, 1913.
[10] H. G. Yang, H. C. Zeng, *J. Phys. Chem. B* **2004**, *108*, 3492.
[11] X. W. Lou, Y. Wang, C. Yuan, J. Y. Lee, L. A. Archer, *Adv. Mater.* **2006**, *18*, 2325.
[12] F. E. Kruis, H. Fissan, A. S. Peled, *J. Aerosol Sci.* **1998**, *29*, 511.
[13] D. Mariotti, R. M. Sankaran, *J. Phys. D: Appl. Phys.* **2010** *43*, 323001.
[14] B. Schimmoeller, S. E. Pratsinis, A. Baiker, *ChemCatChem* **2011**, *3*, 1234.
[15] K. Okuyama, I. W. Lengoro, *Chem. Eng. Sci.* **2003**, *58*, 537.
[16] C. Boissiere, D. Grosso, A. Chaumonnot, L. Nicole, C. Sanchez, *Adv. Mater.* **2011**, *23*, 599.
[17] E. L. Dreizin, *Prog. Energy Combust. Sci.* **2009**, *35*, 141.
[18] D. G. Piercey, T. M. Klapötke, *Cent. Eur. J. Energ. Mater.* **2010**, *7*, 115.
[19] C. Rossi, K. Zhang, D. Estéve, P. Alphonse, P. Thailhades, C. Vahlas, *J. Microelectromech. Syst.* **2007**, *16*, 919.
[20] C. E. Aumann, G. L. Skofronick, J. A. Martin, *J. Vac. Sci. Technol. B* **1995**, *13*, 1178.
[21] S. H. Kim, M. R. Zachariah, *Adv. Mater.* **2004**, *16*, 1821.
[22] J. Y. Malchi, T. J. Foley, R. A. Yetter, *ACS Appl. Mater. Interfaces* **2009**, *1*, 2420.
[23] R. Shende, S. Subramanian, S. Hasan, S. Apperson, R. Thiruvengadathan, K. Gangopadhyay, S. Gangopadhyay, P. Redner, D. Kapoor, S. Nicolich, W. Balas, *Propellants, Explos., Pyrotech.* **2008**, *33*, 239.
[24] F. Séverac, P. Alphonse, A. Estève, A. Bancaud, C. Rossi, *Adv. Funct. Mater.* **2012**, *22*, 323.
[25] K. S. Martirosyan, *J. Mater. Chem.* **2011**, *21*, 9400.
[26] L. Zhou, N. Piekiel, S. Chowdhury, M. R. Zachariah, *J. Phys. Chem. C* **2010**, *114*, 14269.
[27] K. Sullivan, M. R. Zachariah, *J. Propul. Power* **2010**, *26*, 467.
[28] J. M. Amarilla, R. M. Rojas, J. M. Rojo, *J. Power Sources* **2011**,*196*, 5951.
[29] A. Prakash, A. V. McCormick, M. R. Zachariah, *Adv. Mater.* **2005**, *17*, 900.
[30] C. W. Wu, K. Sullivan, S. Chowdhury, G. Q. Jian, L. Zhou, M. R. Zachariah, *Adv. Funct. Mater.* **2012**, *22*, 78.
[31] A. Navrotsky, C. C. Ma, K. Lilova, N. Birkner, *Science* **2010**, *330*, 199.
[32] G. Q. Jian, L. Zhou, N. Piekiel, M. R. Zachariah, presented at *Fall Meeting, the Eastern States Section of the Combustion Institute, Storrs, CT, October, 2011.*